Science Advances
AAAS

advances.sciencemag.org/cgi/content/full/6/13/eaax7547/DC1

Supplementary Materials for

Zero-energy bound states in the high-temperature superconductors at the two-dimensional limit

Chaofei Liu, Cheng Chen, Xiaoqiang Liu, Ziqiao Wang, Yi Liu, Shusen Ye, Ziqiang Wang, Jiangping Hu, Jian Wang*

*Corresponding author. Email: jianwangphysics@pku.edu.cn

Published 25 March 2020, *Sci. Adv.* **6**, eaax7547 (2020)
DOI: 10.1126/sciadv.aax7547

This PDF file includes:

Section S1. Adsorbate-substrate interaction–modulated ZEBS

In our experiments, the Fe adatoms are weakly adsorbed on one-unit-cell (1-UC) FeSe film at the energetically favored hollow sites of surface Se lattice (Fig. 2A and inset of Fig. S1A). Typically, the Fe atoms were deposited with dilute coverage of ~0.002–0.003 monolayer (ML) (e.g., Fig. S1A) (1 ML is defined as the coverage at which Fe adatoms occupy all the hollow sites of surface Se lattice). In statistics, the spins of Fe adatoms are randomly oriented, which locally modulate the magnetic exchange coupling with underlying 1-UC FeSe substrate in different degrees. Thus, the adsorbate–substrate-interaction–dependent Fe-adatom height accordingly appears in a statistical distribution (Fig. S1C). Meanwhile, the energy of the Fe-adatom–induced bound state is similarly distributed (Fig. S1B), yielding a Gaussian profile relatively aligned with adatom-height histogram (Fig. S1, B vs. C). Consequently, the adsorbate–substrate-coupling–tuned bound-state energy for Fe adatom on 1-UC FeSe film is established in statistics. Appropriate exchange interaction between Fe adsorbate and FeSe substrate will pin the bound state at zero energy, which corresponds to a statistical Fe-adatom height of ~62 pm in experiment (Fig. S1C). Particularly, the yielded adatom height for the zero-energy bound state (ZEBS) is relatively large in the Fe-adatom-height histogram (Fig. S1C), suggesting comparably weak adsorbate-substrate interaction. Together with the absence of magnetic-moment extremum at the experimental Fe-adatom height of ~62 pm (Fig. S1D), the adsorbate-substrate coupling for the ZEBS emergence in 1-UC FeSe is evidently below the strong-interaction (unitary) limit.

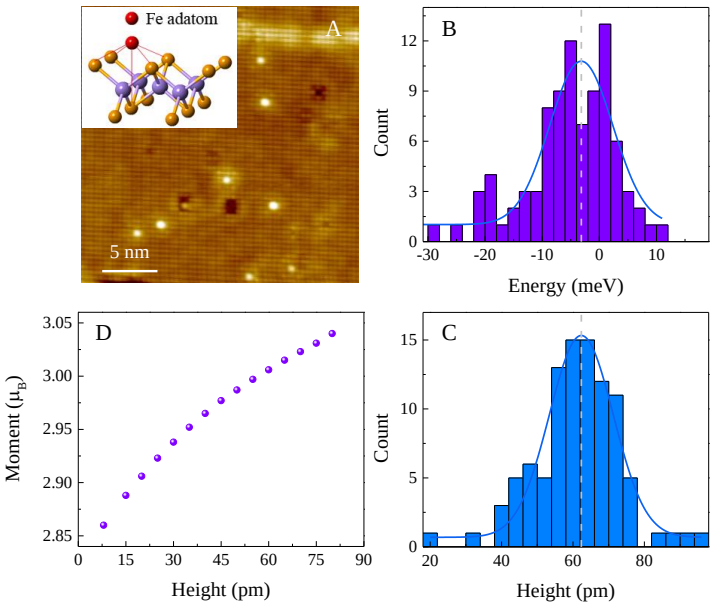

Fig. S1. Statistically correlated bound-state energy and Fe adatom height for 1-UC FeSe. (**A**) Topographic image of Fe adatoms on 1-UC FeSe film (25×25 nm^2; set point: V = 0.2 V, I = 500 pA). Inset: crystal structure of 1-UC FeSe with a Fe adatom centered above the hollow site of four adjacent Se atoms. (**B**,**C**) Bound-state-energy and height statistics for all measured Fe adatoms, both yielding Gaussian distributions (blue curves) with relatively aligned Gaussian-peak positions (dashed lines). The bound state counts for the one with the most intense dI/dV in an individual spectrum. (**D**) Calculated magnetic moment of Fe adatoms on 1-UC FeSe at different heights relative to the upper Se layer (see Materials and Methods). μ_B: Bohr magneton.

Section S2. Additional data of the spatially evolving ZEBS

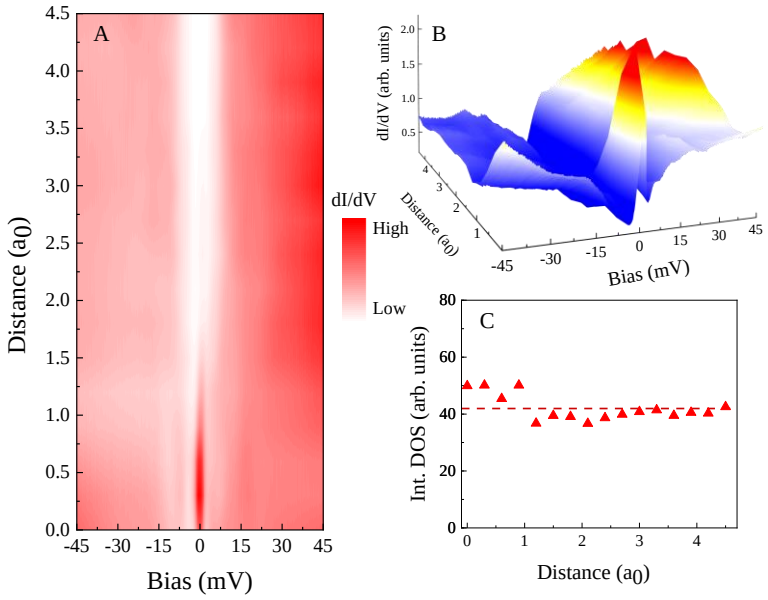

Fig. S2. More analyses of the spatially evolving ZEBS in Fig. 2C. (**A**,**B**) 2D and 3D color plots of the spatially resolved tunneling spectra in Fig. 2C. (**C**) Integrated density of states (DOS) (solid symbols) from −30 to 30 mV for the line spectra in Fig. 2C. The dashed line is the averaged integrated DOS as guide to the eye. The distance in (A)–(C) is defined relative to the Fe-adatom center. (A,B) Set point: V = 0.04 V, I = 2500 pA; modulation: V_{mod} = 1 mV.

Section S3. Fe adatom–reconstructed electronic structures

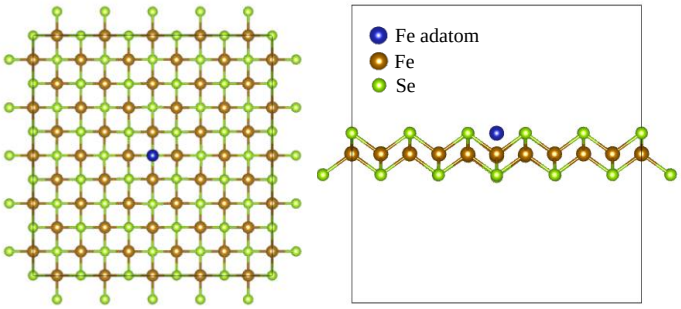

Fig. S3. A 5 × 5 × 1 supercell of 1-UC FeSe with Fe adatom (blue) in the center.

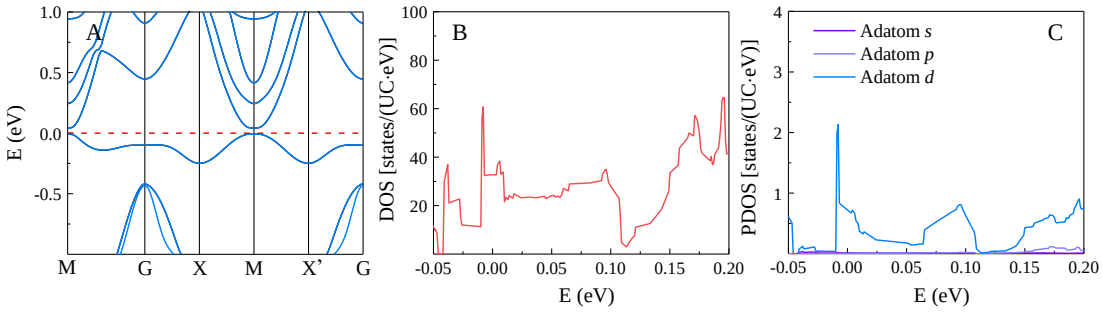

Fig. S4. Electronic structures of 1-UC FeSe reconstructed by Fe adatom. (**A**) Band structures of free-standing 1-UC FeSe with spin-orbit coupling. The $SrTiO_3$ substrate only introduces electron doping in FeSe, which leads to electron Fermi pocket at *M* point. (**B**) DOS for 5 × 5 × 1 1-UC FeSe supercell with Fe adatom. (**C**) DOS projected to Fe adatom. For

calculation details, see Materials and Methods.

Section S4. Prospects for the local ZEBS detection in connate high-temperature superconductors

Compared with the recently prevailing systems hosting the ZEBSs, the 1-UC iron chalcogenides/$SrTiO_3$ *integrate* the desired ingredients for industrially realizing and manipulating ZEBS, which are only partially possessed by individual configurations in previous studies (Table S1; Fig. S5).

(1) *Being connate*. Artificially fabricated Rashba semiconducting nanowires (NWs) (*9*, *10*), spin-textured Fe atomic chains (*11*) and topological-insulator ultrathin films (*12*) in proximity to Bardeen-Cooper-Schrieffer (BCS) superconductors (Table S1) for pursuing the Majorana zero modes (MZMs) often inevitably introduce the interface unambiguity. The extrinsic complexity of configuration interface will hinder a convincing identification of the ZEBS origin. The connate 1-UC FeSe and $FeTe_{0.5}Se_{0.5}$ on $SrTiO_3$ adsorbed by Fe adatoms naturally remove the challenging interface issues.

(2) *High* T_c *and* T_{ZBCP} [T_c: critical temperature of the pristine superconducting (SC) components in MZM configurations; T_{ZBCP}: existing temperature of experimentally detected zero-bias conductance peak (ZBCP)]. In previous literature, experiments engineered the ZEBSs mainly based on proposed configurations in proximity to BCS superconductors (*9*-*12*) and on bulk iron chalcogenide, Fe(Te,Se) (*19*, *20*). Although bulk Fe(Te,Se) is a nominal high-temperature superconductor, its T_c is generally below 15 K (*19*). Therefore, in all previous MZM systems, the generic T_c involved is limited to ~1–10(15) K (Table S1). Further "poisoned" by thermally excited quasiparticles, the MZM-like ZEBS mostly survives at T_{ZBCP} ~0.05–1(4) K (Table S1). As the truly high-T_c [typically 40–65 K (*22*, *24*)] superconductors, 1-UC FeSe and $FeTe_{0.5}Se_{0.5}$ dramatically push T_{ZBCP} up to 10–13 K and 18–20 K, respectively.

(3) *Unnecessity of external magnetic field*. In SC-proximity–coupled semiconducting NWs and p_x+ip_y-wave heterostructures [or bulk Fe(Te,Se)], magnetic field B is required (Table S1) to trigger topological phase transition (*6*) and to generate magnetic vortices to bound the ZEBSs (*8*), respectively. The Fe adatoms on 1-UC FeSe and $FeTe_{0.5}Se_{0.5}$ films intrinsically induce the ZEBSs under zero external B. The unnecessity of magnetic field for inducing the ZEBS in 1-UC iron chalcogenides addresses promising potentials in electronics applications.

Table S1. Summary of the ZEBS-related information in literature. [†for ZBCP-detecting technique; QL: quintuple layer; +: requiring magetic field B].

System	T_c/T_{ZBCP} (K)	B (T)	ξ	Local/Integrated†	Connate/Artificial
Au/InSb-NW/NbTiN (*9*)	12/0.05–0.3	≥0.07	—	Integrated	Artificial
Fe chain/Pb(110) (*11*)	7/1.4	0	~1 nm	Local	Artificial
IFI/Fe_{1+x}(Te,Se) (*19*)	12–14/1.5–15	0	3.5 Å	Local	Connate
Point-contacted Cd_3As_2 (*49*)	≤7.1/0.28–2.8	0	~μm	Local	Artificial
Magnetic vortex/5-QL Bi_2Te_3/$NbSe_2$ (*12*)	7.2/0.03	+	<10 nm	Local	Artificial
Cr-Au/InSb-NW/Al (*10*)	1.3/0.02–0.6	>0.65	—	Integrated	Artificial
Magnetic vortex/$FeTe_{0.55}Se_{0.45}$ (*20*)	14.5/0.55–4.2	+	6 nm	Local	Connate
Fe adatom/1-UC FeSe	65/4–13	0	3.4 Å	Local	Connate
Fe adatom/1-UC $FeTe_{0.5}Se_{0.5}$	62/4–20	0	6.4 Å	Local	Connate

(4) *Short decay length*. The ZEBSs in Fe-atomic-chain ends and vortex centers spatially decay by several

nanometers (*11*, *12*, *20*) (Table S1). Exceptionally, the decay length of the ZEBSs induced by Fe adatoms on both 1-UC FeSe and $FeTe_{0.5}Se_{0.5}$ films is only sub-nanometer (3.4 and 6.4 Å), which is also reported on interstitial iron impurity (IFI) in Fe_{1+x}(Te,Se) bulk material (*19*). Having an advantage over the IFI/Fe_{1+x}(Te,Se) case, the superconductivity in 1-UC FeSe and $FeTe_{0.5}Se_{0.5}$ films is regained with a fully gapped and especially low-bias-DOS–depleted nature instantly away from the Fe adatoms (Fig. 2, C and D; Fig. 4, C and D). The ultralocalized ZEBS and completely recovered SC state within short range in 1-UC iron chalcogenides guarantee the decoupling condition of densely deposited Fe adatoms, making the ZEBS-based high-density information processing (if any) expectable.

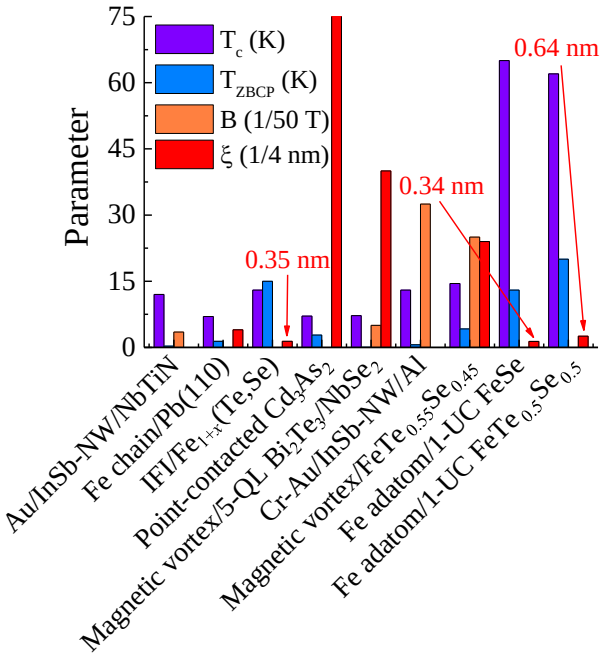

Fig. S5. Histogram of the ZEBS-related parameters in different configurations plotted for direct comparison. Magnetic field *B* in magnetic vortex/5-QL Bi_2Te_3/$NbSe_2$ and magnetic vortex/$FeTe_{0.55}Se_{0.45}$ is drawn by adapting the typical values in original references (*12, 20*). For concrete parameter values, see Table S1.

(5) *Being locally detected and feasibly manipulated*. The SC-proximity–coupled semiconducting NWs as the MZM platforms are measured by the electrical transport, yielding integrated signals (*9*, *10*) (Table S1). Being capable of atomically resolved spectroscopy imaging, the scanning tunneling spectroscopy utilized in the present experiments highlights the advantage of local ZEBS detection. For state manipulation, the intimate entanglement of the MZM-like ZEBSs at two ends of the vortex line in interfacial p_x+ip_y-wave (*12*) and bulk Fe(Te,Se) (*20*) systems appears superfluous. In contrast, the paired-ZEBS entangling is nonexistent in the Fe-adatom situation due to the ideal two-dimensionality of 1-UC iron chalcogenides. The technically feasible atomic-manipulation technique by using scanning-tunneling-microscope tip further drives the systems of Fe-adatom/1-UC iron chalcogenides towards applicable quantum-functionality electronics.